Transient Stability Impact of Reactive Power Control on Grid-Connected Converters

Pan, Donghua; Wang, Xiongfei; Liu, Fangcheng; Shi, Rongliang

Published in:
2019 IEEE Energy Conversion Congress and Exposition, ECCE 2019

DOI (link to publication from Publisher):
10.1109/ECCE.2019.8912567

Publication date:
2019

Document Version
Accepted author manuscript, peer reviewed version

Transient Stability Impact of Reactive Power Control on Grid-Connected Converters

Donghua Pan
Dept. of Energy Technology
Aalborg University
Aalborg, Denmark
dop@et.aau.dk

Xiongfei Wang
Dept. of Energy Technology
Aalborg University
Aalborg, Denmark
xwa@et.aau.dk

Fangcheng Liu
Central Research Institute
Huawei Technologies Co., Ltd.
Shanghai, China
formula.liu@huawei.com

Rongliang Shi
Central Research Institute
Huawei Technologies Co., Ltd.
Shanghai, China
shirongliang@huawei.com

***Abstract*—This paper presents a design-oriented transient stability analysis of a droop-controlled voltage-source converter (VSC), where the effect of reactive power control is in focus. By looking into the dynamic coupling between the active power loop and the reactive power loop, a large-signal model of the droop controller is built first. Based on this model, the transient responses of the droop-controlled VSC under grid faults are then evaluated using the phase portrait. It reveals that the reactive power control will generate a transient voltage drop to the VSC, which takes a positive feedback effect and deteriorates the transient stability. Fortunately, such a voltage drop can be offset by raising the reactive power reference. Finally, simulations and experiments are performed to verify the theoretical analysis.**

***Index Terms*—Droop control, large-signal disturbance, reactive power control, transient stability, voltage-source converter.**

I. Introduction

Voltage-source converters (VSCs) are widely used in modern power grids for renewable energy generations and energy-saving applications [1]–[4]. To regulate the exchange of active and reactive powers with the grid, the *P-f* and *Q-V* droop control is usually employed in the VSCs [5], [6]. Substantial research efforts have been devoted to the stability analysis of the droop-controlled VSC, with the main focus on the small-signal disturbance [7], [8]. However, if a large-signal disturbance happens, e.g., a fault on transmission lines, a severe grid voltage sag, and a large load swing, the *transient stability* of the VSC, which characterizes the ability of the VSC to maintain synchronization with the grid [9], is concerned, and it attracts increasing research interests recently. In [10] and [11], a transient instability phenomenon of the droop-controlled VSC is found in the case of a current saturation due to a grid voltage sag. The similar phenomenon is also predicted in [12] by means of the deep learning theory. In [13], a VSC with the power-synchronization control (an equivalence to the droop control [14], [15]) is studied, and its transient behavior is explored in different types of grid faults.

In those works, the transient stability is believed to be merely determined by the active power control (the *P-f* droop), whereas the effect of the reactive power control (the *Q-V* droop) is overlooked. In fact, these two control loops are coupled with each other. For example, the reactive power loop commands the voltage amplitude of the VSC, which, in turn, rescales the active power delivered to the grid. Due to this coupling effect, the reactive power control will also have an impact on the transient stability of the VSC, which is however not revealed yet.

This paper attempts to fill this gap by identifying the role that the reactive power control plays in the transient behavior of the droop-controlled VSC. To begin with, a large-signal model of the droop controller considering the coupling effect is developed in Section II. Based on this model, the VSC without a reactive power control is discussed at first to help understand the basic concept of the transient stability. This is followed by an insight into the effect of the reactive power control in Section III. It is shown that the reactive power control generates a visible voltage drop to the VSC during a transient process. Such a voltage drop will introduce a *positive feedback* effect and thus deteriorate the transient stability. To address this issue, the voltage drop is compensated by raising the reactive power reference. These theoretical expectations are confirmed by simulations and experimental results in Section IV, before drawing the conclusion in Section V.

II. Concept of Transient Stability in Grid-Connected Converter

A. System Description and Modeling

Fig. 1 illustrates a VSC feeding into the grid through a transformer and two-paralleled transmission lines. A constant dc voltage V_{in} is assumed at the input of the VSC. Inductor L_f and capacitor C_f form an output filter of the VSC, which is actually an *LCL* filter considering the grid inductance [16]–[18]. X_T and X_L are the transformer leakage reactance and the line reactance, respectively. From the point of common coupling (PCC), the grid can be seen as an equivalent reactance X_g in series with a voltage source (vector) **E** which has a constant amplitude E and a constant frequency ω_0.

The VSC is controlled as a grid-forming voltage source by the well-known *P-f* and *Q-V* droop method [5], [6], i.e.,

$$\omega = \omega_0 + K_{\text{pf}}\left(P_0 - P\right) \tag{1}$$

$$V = V_0 + K_{\text{qv}}\left(Q_0 - Q\right) \tag{2}$$

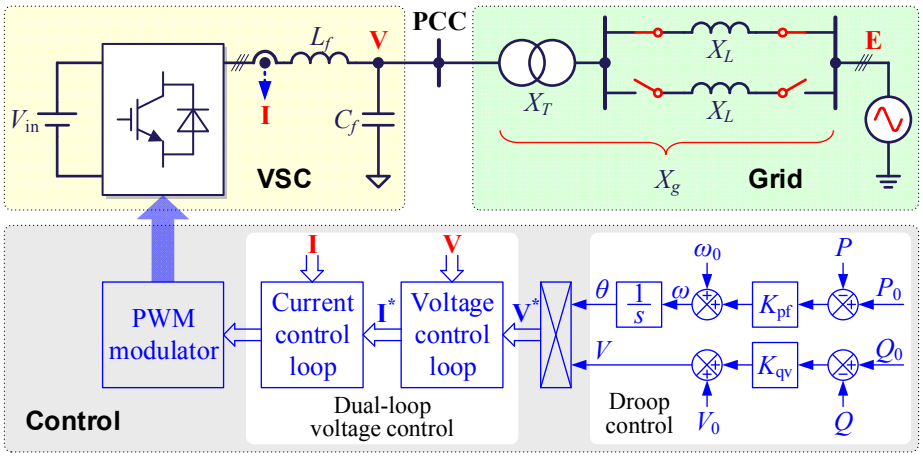

Fig. 1. Configuration of a droop-controlled VSC connected to the grid.

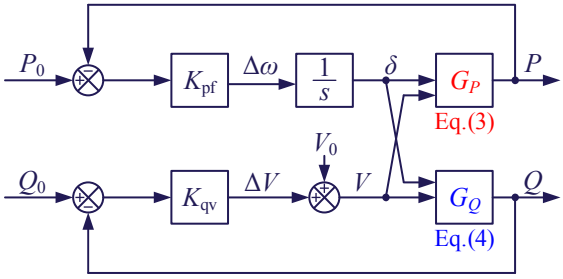

Fig. 2. Large-signal model of the power control loops.

where ω and V are the frequency and amplitude of the VSC output voltage, with ω_0 and V_0 being their references; P and Q are the active and reactive powers, with P_0 and Q_0 being their references; and K_{pf} and K_{qv} are the P-f and Q-V droop gains.

As shown in Fig. 1, ω is processed by a pure integrator to obtain the phase θ, which together with V, generates the voltage reference vector $\mathbf{V}^*$. The output voltage vector $\mathbf{V}$ is regulated by a voltage loop to track this reference. A current loop is cascaded to the voltage loop to damp the LC resonance and thus enhance the system stability [7], [8]. Generally, the dynamic of the outer power loop is over a decade slower than that of the inner voltage & current loop [19]. The outer loop and the inner loop can thus be evaluated individually. Hence, when analyzing the transient stability issue caused by the outer power loop, the inner dual-loop voltage control can be regarded as a unity gain with an ideal reference tracking [10]–[13], i.e., $\mathbf{V} = \mathbf{V}^*$ and $|\mathbf{V}| = V$.

Taking the voltage vector $\mathbf{E}$ as a reference and assuming the phase difference between $\mathbf{V}$ and $\mathbf{E}$ is δ, i.e., the power angle, we can obtain $\mathbf{E} = E\angle 0$ and $\mathbf{V} = V\angle\delta$. Thus, P and Q from the PCC can be expressed as [9]

$$P = \frac{3}{2}\cdot\frac{EV\sin\delta}{X_g} \tag{3}$$

$$Q = \frac{3}{2}\cdot\frac{V^2 - EV\cos\delta}{X_g}. \tag{4}$$

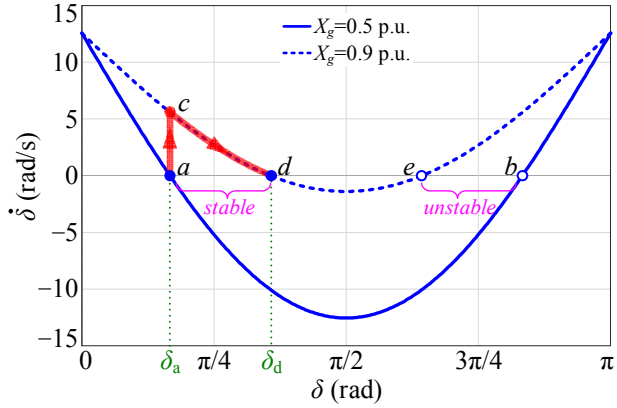

Fig. 3. Phase portraits without the reactive power control ($V = V_0$).

Obviously, both P and Q are related to δ and V, which means that the active power loop that commands δ and the reactive power loop that commands V interact with each other. Considering this interaction, a large-signal model of the power control loop is obtained, as shown in Fig. 2, where G_P and G_Q are the expressions of P and Q, i.e., (3) and (4), respectively.

B. Transient Stability Analysis with Phase Portrait

Generally, the transient stability of the VSC is dependent on the dynamic response of δ under a large disturbance (usually a grid fault). To illustrate the basic concept of the transient stability, the reactive power control is not considered first and V is assumed to be a constant V_0. Recalling (3) and Fig. 2, letting $V = V_0$, the frequency deviation $\Delta\omega$, which is the derivative of δ, is obtained as

$$\begin{aligned}\dot{\delta} &= K_{pf}\left(P_0 - P\right)\\ &= K_{pf}\left(P_0 - \frac{3}{2}\cdot\frac{EV\sin\delta}{X_g}\right) = K_{pf}\left(P_0 - \frac{3}{2}\cdot\frac{EV_0\sin\delta}{X_g}\right).\end{aligned} \tag{5}$$

In the steady-state, the VSC operates at the grid frequency ω_0, thus $\Delta\omega = \dot{\delta} = 0$ and $P = P_0$. This operating point can be identified by the $\dot{\delta}$-δ curve, which is the so-called phase portrait [20]. With the phase portrait, the change of δ can be

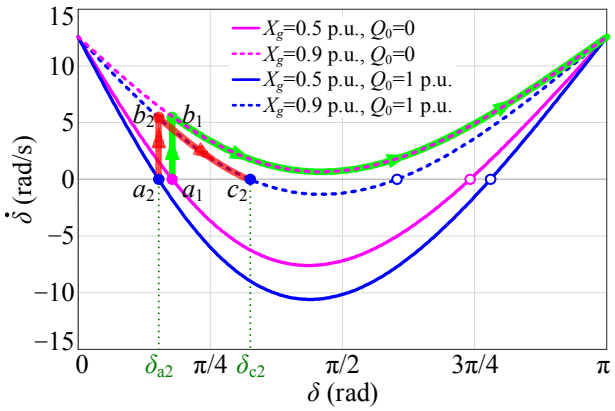

Fig. 4. Phase portraits with the reactive power control.

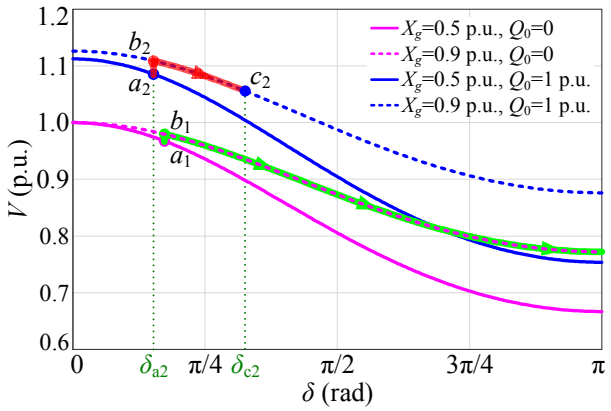

Fig. 5. V-δ curves with the reactive power control.

readily predicted, i.e., δ will increase if $\dot{\delta} > 0$ and decrease if $\dot{\delta} < 0$, and $\dot{\delta} = 0$ corresponds to the equilibrium points. According to the parameters in Table I, the phase portrait with both transmission lines in service (i.e., $X_g = 0.5$ p.u.) is plotted with the solid line in Fig. 3. There are two equilibrium points, where point a (the solid dot) is the stable one, since δ can return to this point irrespective of a small disturbance; while point b (the open circle) is the unstable one, since a small disturbance will force δ to departure from this point. Thus, the VSC operates at point a with a power angle of δ_a.

The transient stability issue arises if P is subjected to a sharp drop, which can result from a notable increase of X_g. For example, if one of the transmission lines is disconnected due to a three-phase open-circuit fault (see Fig. 1), the effective X_g becomes higher (0.9 p.u.), leading to a higher phase portrait, shown as the dashed line in Fig. 3. At the fault occurring instant, δ_a is held while the operating point jumps from a to c. Then, δ starts to increase due to $\dot{\delta} > 0$, which drives the operating point from c to d. Once reaching point d, a new steady state is achieved due to $\dot{\delta} = 0$, and the power angle stops at δ_d. From the above analysis, it can be found that due to the first-order dynamic behavior of δ [see (5)], the VSC can retain a stable operation if $\dot{\delta} = 0$ ($P = P_0$) is reached, where an equilibrium point exists, after a transient process.

III. Effect of Reactive Power Control on Transient Stability

In the previous analysis, the VSC output voltage V is assumed to hold a constant amplitude V_0 by ignoring the reactive power control. However, in practice, both the active power P and the reactive power Q are varied under a large disturbance. The varied Q will alter V according to the Q-V droop law, which will, in turn, change P and then affect the transient stability.

To quantify this effect, we first rewrite the Q-V droop law by substituting (4) into (2), i.e.,

$$V = V_0 + K_{qv}\left(Q_0 - \frac{3}{2}\cdot\frac{V^2 - EV\cos\delta}{X_g}\right) \tag{6}$$

which is obviously a quadratic equation of V. Solving this equation, V is found related to δ by (7). Thus, the dynamic equation of δ, considering the effect of reactive power control, can be described as (8), shown at the bottom of this page.

Based on (8), the phase portraits are plotted in Fig. 4 with the same parameters in Table I. It is clear that for $Q_0 = 0$, the system trajectory (indicated with arrows) starts at point a_1 before the fault ($X_g = 0.5$ p.u.), and jumps to point b_1 when the fault occurs ($X_g = 0.9$ p.u.), then diverges to infinite as $\dot{\delta} > 0$ always holds (no equilibrium point). This indicates a poorer transient stability than the case shown in Fig. 3 where $V = V_0$.

To figure out the reason, the V-δ curves are drawn based on (7), as shown in Fig. 5. At the fault occurring instant, as X_g increases suddenly, Q drops sharply referring to (4), which causes V to jump from point a_1 to point b_1. Then, as δ increases, Q also increases according to (4), which causes V to drop according to the Q-V droop law. The voltage drop will degrade P referring to (3), which will, in turn, enlarge $\dot{\delta}$ and force δ to increase further, and then push V to drop deeper, shown as the trajectory with arrows. Hence, the reactive power loop inherently introduces a "positive feedback" effect

$$V = \frac{1.5K_{qv}E\cos\delta - X_g + \sqrt{\left(X_g - 1.5K_{qv}E\cos\delta\right)^2 + 6K_{qv}X_g\left(V_0 + K_{qv}Q_0\right)}}{3K_{qv}}. \tag{7}$$

$$\dot{\delta} = K_{pf}\left(P_0 - \frac{3}{2}\cdot\frac{EV\sin\delta}{X_g}\right) = K_{pf}\left(P_0 - \frac{3}{2}\cdot\frac{E\sin\delta}{X_g}\cdot\frac{1.5K_{qv}E\cos\delta - X_g + \sqrt{\left(X_g - 1.5K_{qv}E\cos\delta\right)^2 + 6K_{qv}X_g\left(V_0 + K_{qv}Q_0\right)}}{3K_{qv}}\right). \tag{8}$$

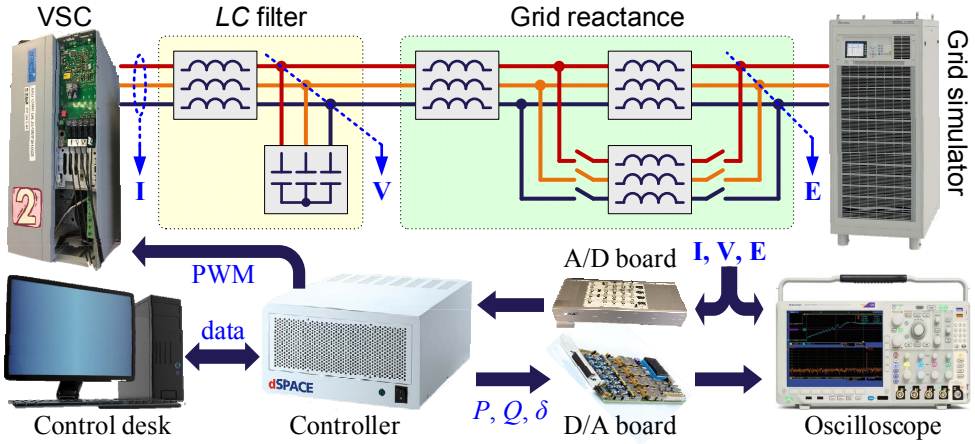

Fig. 6. Configuration of the experimental setup.

on the transient response. Consequently, the transient stability with the reactive power loop is deteriorated.

To avoid the transient instability, the voltage drop caused by the reactive power control needs to be compensated, which can be achieved by raising Q_0. Recalling (7), it can be found that V increases monotonically with the increase of Q_0. The minimum required Q_0 depends on the depth of voltage drop. The more V drops, the larger Q_0 is required. Taking $Q_0 = 1$ p.u. as an instance, the V-δ curves move upward holistically, which thus offset the voltage drop, as shown in Fig. 5. The offset V helps to restore P and then push the phase portrait lower to 0. Accordingly, as highlighted in Figs. 4 and 5, the system trajectory now moves from point a_2 to point b_2 and finally stops at point c_2, where a new steady state is reached.

IV. Simulation and Experimental Results

To verify the theoretical analysis on the transient stability, time-domain simulations and experimental tests are carried out in this section. Fig. 6 shows the configuration of the experimental setup. The VSC is implemented by a Danfoss VLT FC-103P11K inverter, whose input is supplied by a constant dc voltage source, and its output is connected with an LC filter. Three-phase inductors are used to emulate the transformer leakage reactance X_T and the line reactance X_L. The Chroma 61845 grid simulator is employed to provide the grid voltage **E**. The VSC output voltage **V** and VSC output current **I** are measured through the dSPACE DS2004 A/D board. The measured signals are sent to the dSPACE DS1007 platform to implement the outer power control and the inner dual-loop voltage control. The phase angles of **V** and **E** are measured by a fast phase-locked loop, and their phase difference, which is denoted as the power angle δ, is fed to the oscilloscope through the dSPACE DS2102 D/A board.

The same parameters are used with both the simulations and experimental tests, as listed in Table I, where L_T and L_L are the inductances yielding X_T and X_L, i.e., $X_T = \omega_0 L_T$ and $X_L = \omega_0 L_L$. A low grid voltage $E = 100$ V is intentionally chosen for the convenience of emulating the low short-circuit-ratio grid condition. The droop gains K_{pf} and K_{qv} are designed according to the allowed frequency deviation $\Delta\omega$ under the maximum active power P_{max} and the allowed voltage deviation ΔV under the maximum reactive power Q_{max}, respectively [5], [6]. For the grid-connected application, the VSC can inject the full active power or the full reactive power depending on the operating scenarios. Hence, $P_{max} = Q_{max} = 1$ p.u.. Meanwhile, $\Delta\omega = 0.04\omega_0$ and $\Delta V = 0.15V_0$ are set, which give rise to $K_{pf} = 0.04\omega_0/P_{max}$ and $K_{qv} = 0.15V_0/Q_{max}$, respectively. Based on these parameters, transient responses of the VSC are examined in the case of the open-circuit fault on one transmission line. Obviously, $X_g = X_T + X_L/2 = 0.5$ p.u. before the fault, and $X_g = X_T + X_L = 0.9$ p.u. after the fault.

TABLE I. Parameters for Simulation and Experimental Tests

Parameter	Value	p.u.	Parameter	Value	p.u.
Rated power P_0	2 kW	1.0	Filter inductance L_f	1.5 mH	0.06
Rated voltage V_0	100 V	1.0	Filter capacitance C_f	20 μF	0.05
Grid voltage E	100 V	1.0	Leakage inductance L_T	2.5 mH	0.1
Grid frequency ω_0	314 rad/s		Line inductance L_L	19 mH	0.8
P-f droop gain K_{pf}	$0.04\omega_0/P_{max}$	0.04	Q-V droop gain K_{qv}	$0.15V_0/Q_{max}$	0.15

First, by disabling the reactive power control and setting $V = V_0$, a simulated result is acquired, as shown in Fig. 7(a). When the open-circuit fault occurs, δ starts to increase gradually until reaching a new steady state. The power angles before and after the fault are 30° and 64°, respectively, which correspond to δ_a and δ_d in Fig. 3. The VSC output voltage is kept constant as expected, while its output current is slightly lifted because of the raised reactive power caused by the increased δ. No oscillation is observed during the transient process, which implies a strong transient stability.

Then, the reactive power control is enabled, and the corresponding simulation result is given in Fig. 7(b). With $Q_0 = 0$, an unstable transient response is triggered by the open-circuit fault, and low-frequency oscillations are observed in all the waveforms of P, Q, δ, V, and I, which implies a loss

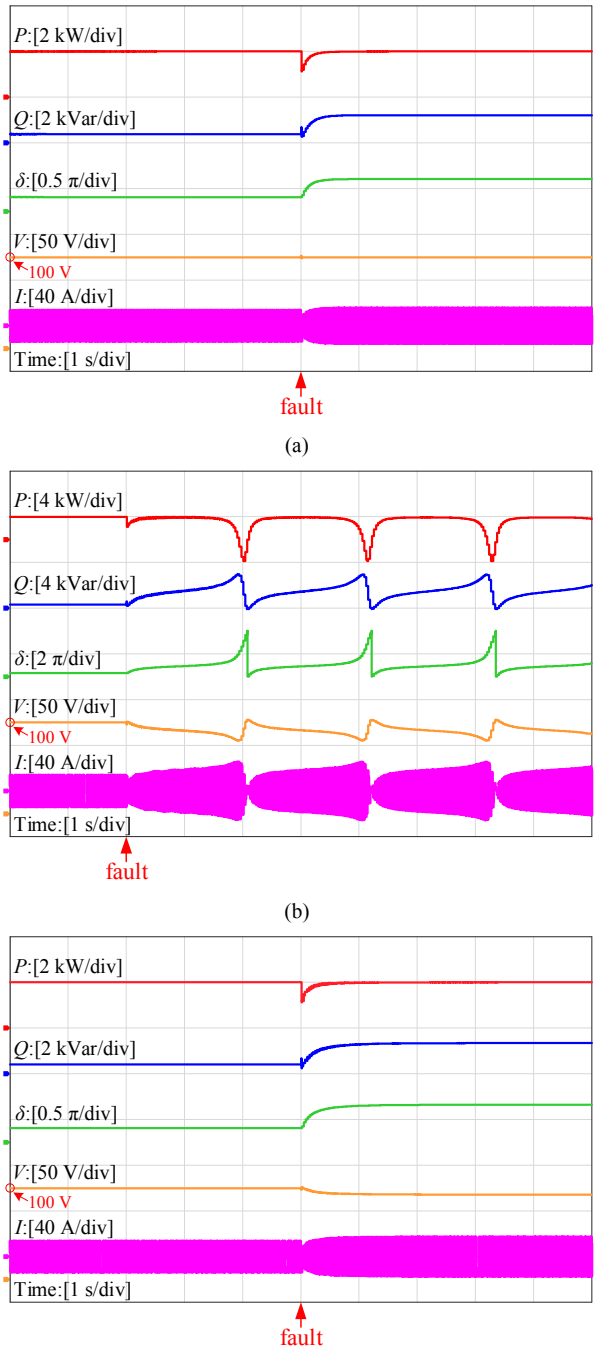

Fig. 7. Simulated transient responses of the droop-controlled VSC. (a) Without the reactive power control, $V = V_0$. (b) With the reactive power control, $Q_0 = 0$. (c) With the reactive power control, $Q_0 = 0.25$ p.u..

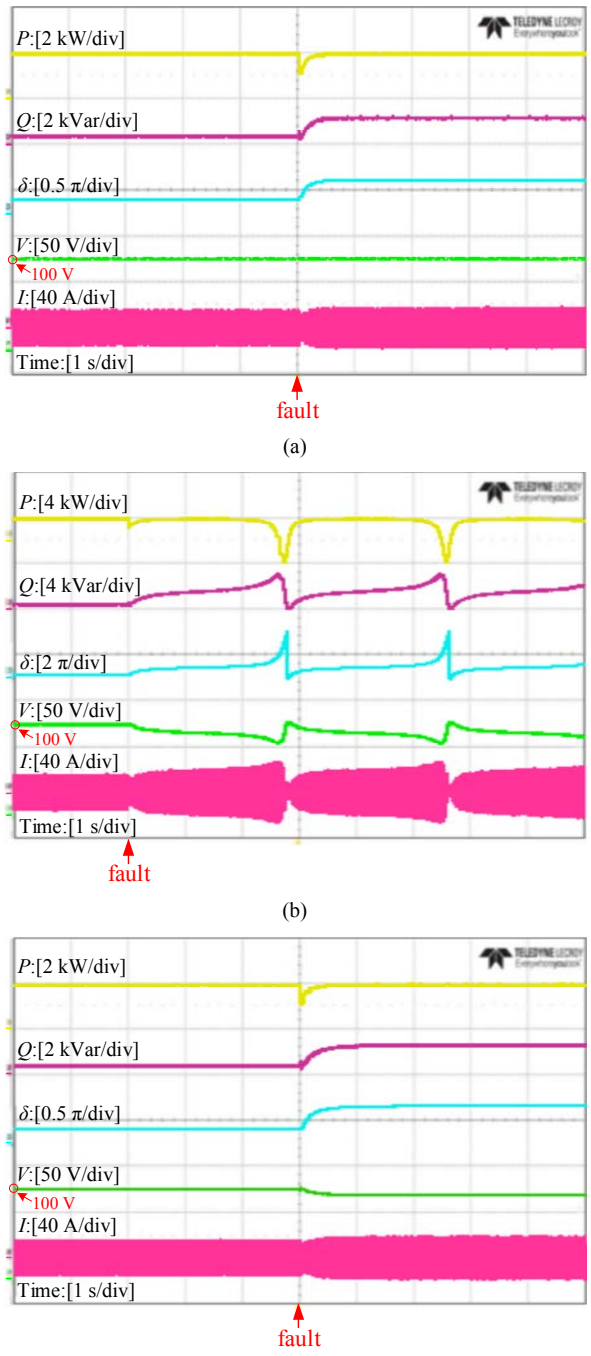

Fig. 8. Experimental transient responses of the droop-controlled VSC. (a) Without the reactive power control, $V = V_0$. (b) With the reactive power control, $Q_0 = 0$. (c) With the reactive power control, $Q_0 = 0.25$ p.u..

of the synchronization with the grid. To restore the grid synchronization, a proper Q_0 is suggested in Section III. Here, $Q_0 = 0.25$ p.u. is taken as an instance. As shown in Fig. 7(c), a stable transient response is recovered. The VSC is transferred to a new steady state with δ being raised from 30º to 75º smoothly, and V is slightly dropped with the raised Q after the fault. The simulation results confirm the theoretical analysis on the reactive power control.

Fig. 8 shows the experimental results under a sudden disconnection of one transmission line. When the reactive power control is disabled, a stable transient response is observed, and the VSC voltage amplitude V is kept constant at the target value $V_0 = 100$ V, as shown in Fig. 8(a). When the reactive power control is enabled and $Q_0 = 0$ is set, low-frequency oscillations are triggered in the measured P, Q, δ, V, and I, as shown in Fig. 8(b). Compared with the simulation

results in Fig. 7(b), the experimental waveforms show a relatively longer oscillation period. This is due to the extra damping of parasitic resistors in the experimental setup (not modeled in simulation), which slows down the system dynamic responses. Then, by raising Q_0 to 0.25 p.u., a stable operation is restored, as shown in Fig. 8(c). It is obvious that the experimental results are in agreement with the simulation results and the theoretical analysis.

V. Conclusions

This paper has explored the effect of reactive power control on the transient stability of the droop-controlled VSC. A large-signal model that accounts for the coupling between the active power loop and the reactive power loop has been developed for the droop controller. Based on this model, the transient behavior of the droop-controlled VSC is quantified by a first-order nonlinear differential equation and then evaluated with the phase portrait. It has been found that owing to the transient voltage drop resulted from the reactive power control, a positive feedback effect is imposed on the VSC transient response, and its transient stability is deteriorated. This negative effect can be alleviated by raising the reactive power reference. All the theoretical findings have been corroborated by simulations and experimental results.

References

[1] J. Rocabert, A. Luna, F. Blaabjerg, and P. Rodríguez, "Control of power converters in AC microgrids," *IEEE Trans. Power Electron.*, vol. 27, no. 11, pp. 4734−4749, Nov. 2012.

[2] D. Pan, X. Ruan, C. Bao, W. Li, and X. Wang, "Capacitor-current-feedback active damping with reduced computation delay for improving robustness of *LCL*-type grid-connected inverter," *IEEE Trans. Power Electron.*, vol. 29, no. 7, pp. 3414−3427, Jul. 2014.

[3] D. Pan, X. Ruan, C. Bao, W. Li, and X. Wang, "Optimized controller design for *LCL*-type grid-connected inverter to achieve high robustness against grid-impedance variation," *IEEE Trans. Ind. Electron.*, vol. 62, no. 3, pp. 1537−1547, Mar. 2015.

[4] D. Pan, X. Ruan, X. Wang, H. Yu, and Z. Xing, "Analysis and design of current control schemes for *LCL*-type grid-connected inverter based on a general mathematical model," *IEEE Trans. Power Electron.*, vol. 32, no. 6, pp. 4395−4410, Jun. 2017.

[5] Y. W. Li, D. M. Vilathgamuwa, and P. C. Loh, "Design, analysis, and real-time testing of a controller for multibus microgrid system," *IEEE Trans. Power Electron.*, vol. 19, no. 5, pp. 1195−1204, Sep. 2004.

[6] Y. W. Li and C.-N. Kao, "An accurate power control strategy for power-electronics-interfaced distributed generation units operating in a low-voltage multibus microgrid," *IEEE Trans. Power Electron.*, vol. 24, no. 12, pp. 2977−2988, Dec. 2009.

[7] E. A. A. Coelho, P. C. Cortizo, and P. F. D. Garcia, "Small-signal stability for parallel-connected inverters in stand-alone AC supply systems," *IEEE Trans. Ind. Appl.*, vol. 38, no. 2, pp. 533−542, Mar./Apr. 2002.

[8] N. Pogaku, M. Prodanović, and T. C. Green, "Modeling, analysis and testing of autonomous operation of an inverter-based microgrid," *IEEE Trans. Power Electron.*, vol. 22, no. 2, pp. 613−625, Mar. 2007.

[9] P. Kundur, *Power System Stability and Control*. New York, NY, USA: McGraw-Hill, 1994.

[10] H. Xin, L. Huang, L. Zhang, Z. Wang, and J. Hu, "Synchronous instability mechanism of P-f droop-controlled voltage source converter caused by current saturation," *IEEE Trans. Power Syst.*, vol. 31, no. 6, pp. 5206−5207, Nov. 2016.

[11] L. Huang, H. Xin, Z. Wang, L. Zhang, K. Wu, and J. Hu, "Transient stability analysis and control design of droop-controlled voltage source converters considering current limitation," *IEEE Trans. Smart Grid*, vol. 10, no. 1, pp. 578−591, Jan. 2019.

[12] X. Yu, F. Gao, and G. Ding, "Deep learning based transient stability assessment for grid-connected inverter," in *Proc. IEEE International Power Electronics and Application Conference and Exposition (PEAC)*, Shenzhen, China, Nov. 2018.

[13] H. Wu and X. Wang, "Design-oriented transient stability analysis of grid-connected converters with power synchronization control," *IEEE Trans. Ind. Electron.*, vol. 66, no. 8, pp. 6473−6482, Aug. 2019.

[14] L. Zhang, L. Harnefors, and H.-P. Nee, "Power-synchronization control of grid-connected voltage-source converters," *IEEE Trans. Power Syst.*, vol. 25, no. 2, pp. 809−820, May 2010.

[15] L. Zhang, L. Harnefors, and H.-P. Nee, "Interconnection of two very weak AC systems by VSC-HVDC links using power-synchronization control," *IEEE Trans. Power Syst.*, vol. 26, no. 1, pp. 344−355, Feb. 2011.

[16] D. Pan, X. Ruan, C. Bao, W. Li, and X. Wang, "Magnetic integration of the *LCL* filter in grid-connected inverters," *IEEE Trans. Power Electron.*, vol. 29, no. 4, pp. 1573− 1578, Apr. 2014.

[17] D. Pan, X. Ruan, and X. Wang, "Direct realization of digital differentiators in discrete domain for active damping of *LCL*-type grid-connected inverter," *IEEE Trans. Power Electron.*, vol. 33, no. 10, pp. 8461−8473, Oct. 2018.

[18] D. Pan, X. Ruan, X. Wang, F. Blaabjerg, X. Wang, and Q. Zhou, "A highly robust single-loop current control scheme for grid-connected inverter with an improved *LCCL* filter configuration," *IEEE Trans. Power Electron.*, vol. 33, no. 10, pp. 8474−8487, Oct. 2018.

[19] H. Yuan, X. Yuan, and J. Hu, "Modeling of grid-connected VSCs for power system small-signal stability analysis in DC-link voltage control timescale," *IEEE Trans. Power Syst.*, vol. 32, no. 5, pp. 3981−3991, Sep. 2017.

[20] S. H. Strogatz, *Nonlinear Dynamics and Chaos: With Applications to Physics, Biology, Chemistry, and Engineering*, 2nd ed. Boca Raton, FL, USA: CRC Press, 2018.